

Role of turbulence fluctuations on uncertainties of acoustic Doppler current profiler discharge measurements

Leticia Tarrab,¹ Carlos M. García,¹ Mariano I. Cantero,³ and Kevin Oberg²

Received 21 July 2011; revised 20 February 2012; accepted 17 April 2012; published 6 June 2012.

[1] This work presents a systematic analysis quantifying the role of the presence of turbulence fluctuations on uncertainties (random errors) of acoustic Doppler current profiler (ADCP) discharge measurements from moving platforms. Data sets of three-dimensional flow velocities with high temporal and spatial resolution were generated from direct numerical simulation (DNS) of turbulent open channel flow. Dimensionless functions relating parameters quantifying the uncertainty in discharge measurements due to flow turbulence (relative variance and relative maximum random error) to sampling configuration were developed from the DNS simulations and then validated with field-scale discharge measurements. The validated functions were used to evaluate the role of the presence of flow turbulence fluctuations on uncertainties in ADCP discharge measurements. The results of this work indicate that random errors due to the flow turbulence are significant when: (a) a low number of transects is used for a discharge measurement, and (b) measurements are made in shallow rivers using high boat velocity (short time for the boat to cross a flow turbulence structure).

Citation: Tarrab, L., C. M. García, M. I. Cantero, and K. Oberg (2012), Role of turbulence fluctuations on uncertainties of acoustic Doppler current profiler discharge measurements, *Water Resour. Res.*, 48, W06507, doi:10.1029/2011WR011185.

1. Introduction

[2] Acoustic Doppler technologies, in particular acoustic Doppler velocimeters and acoustic Doppler current profilers (ADVs and ADCPs hereafter), are used worldwide to measure discharge in inland waterways and estuaries [Oberg *et al.*, 2005; Oberg and Mueller, 2007]. For discharge measurements made using ADCPs from moving boats under approximately steady flow conditions, it is common practice to collect four or more cross-sectional transects made in reciprocal (opposite) directions and to report the average of the four (or more) discharges as the measured discharge. A transect is a series of successive vertical profiles acquired across the stream. Many factors affect the uncertainty of ADCP discharge measurements, such as measurement location, velocity fluctuations due to flow turbulence, flow unsteadiness, instrument configuration,

and instrument signal processing techniques. Thus, random errors of ADCP discharge measurements from moving boats include error contributions from all the processes present during the flow field sampling (for example, instrument noise, environmental noise, and flow turbulence). The term “instrument noise” is used to refer to electronic noise, the term “environmental noise” is used to refer to the effect measuring conditions have on instrument performance, e.g., wake turbulence, surface waves, and Doppler noise, and the term “flow turbulence” is used to refer to the turbulence generated by flow/bed interaction. Even measurements obtained using an ideal instrument (one that has no electronic noise and that is not adversely affected by measurement conditions) will have random errors because of turbulent fluctuations in the flow. An ADCP cannot simultaneously sample the instantaneous flow field through an entire cross section. ADCPs measurements are typically made by moving a boat with an ADCP across a cross section at a speed that is less than or equal to the mean water velocity. As the boat and ADCP move through the cross section, different turbulent structures moving with the flow are sampled by the ADCP, generating turbulence fluctuations in the mean flow velocity field. The purpose of this work is to quantify the role of “flow turbulence fluctuations” on ADCP discharge measurement uncertainties. Specifically, this analysis addresses the relative importance that spatial- and temporal-sampling strategies (e.g., exposure time, number of sampled transects, instrument sampling frequency) and the existing flow conditions (e.g., mean flow velocity, water depth, and river width) have on the contribution of “flow turbulence” to ADCP discharge measurement uncertainties. The results presented in this work are for moving-boat ADCP discharge measurements; mid- or mean-section discharge measurements are not addressed.

¹Consejo Nacional de Investigaciones Científicas y Técnicas (CONICET), Centro de Estudios y Tecnología del Agua, Facultad de Ciencias Exactas, Físicas y Naturales, Universidad Nacional de Córdoba, Av. Filloy s/n, Ciudad Universitaria, Córdoba, Argentina.

²Consejo Nacional de Investigaciones Científicas y Técnicas (CONICET), Centro Atómico Bariloche, Comisión Nacional de Energía Atómica, Instituto Balseiro, Universidad Nacional de Cuyo, Bustillo, San Carlos de Bariloche, Río Negro, Argentina.

³U.S. Geological Survey, Office of Surface Water, Urbana, Illinois, USA.

Corresponding author: C. M. García, Consejo Nacional de Investigaciones Científicas y Técnicas (CONICET), Centro de Estudios y Tecnología del Agua, Facultad de Ciencias Exactas, Físicas y Naturales, Universidad Nacional de Córdoba, Av. Filloy s/n, Ciudad Universitaria, Córdoba, Argentina. (cgarcia2mjc@gmail.com)

[3] Dimensional analysis and direct numerical simulation (DNS) are used to develop equations for quantifying the uncertainty in ADCP discharge measurements due to flow turbulence. Dimensional analysis has been used to identify relevant dimensionless groups for establishing a functional relationship. Two dimensionless parameters for quantifying the uncertainty in discharge measurements were identified: the relative variance, $RVar[Q]$ and the relative maximum expected error $RME[Q]$. Functional forms of equations for defining $RVar[Q]$ and $RME[Q]$ are obtained by sampling DNS-generated flow data. DNS presents an ideal tool for a systematic analysis to quantify the role of turbulence on uncertainties of ADCP discharge measurements. Namely, using DNS, a detailed data set can be created in which the contributions due to the presence of flow turbulence can be isolated (any experimental data set will include noise intrinsic to the selected technique). DNS also solves for all relevant time and length scales present in the flow with no need for turbulence closure schemes, providing high resolution flow field data (both spatially and temporally) needed for the uncertainty analysis [Garcia *et al.*, 2005] performed in this paper. Although DNS can hardly be applied to field-scale flows, the levels of turbulence attained at moderate Reynolds number flows, where DNS is feasible, are representative of mature turbulent flows. Based on Reynolds invariance, the results can be extrapolated, with some caution, to larger Reynolds-number flows. Reynolds invariance involves that dimensionless characteristics of the developed turbulent flow; i.e., turbulent intensity, mean velocity, etc., are independent of the Reynolds number [Abe *et al.*, 2001]. The DNS simulation was performed for a moderate bulk Reynolds number of the flow and was validated with experimental results available in the literature. Then, the simulated three-dimensional instantaneous flow field was sampled by modeling the ADCP sampling strategies to assess the uncertainty in the measurement of a turbulent flow field as reported by these instruments.

[4] The equations developed using dimensional analysis and DNS were verified with field data from two rivers having differing flow characteristics. Detailed analyses were performed to select the best set of available data to be used for the validation, i.e., data sets in which the contributions of other processes present during the measurement (i.e., instrument noise and environmental noise) are minimized. The findings of this work are useful to define the relative contribution of one of the random processes present during the discharge measurement using an ADCP.

2. Dimensional Analysis

[5] The dimensionless parameters quantifying the uncertainty in discharge measurements (either $RVar[Q]$ or $RME[Q]$) can be estimated using information related to the existing flow conditions during the measurement and the selected sampling configuration. The existing turbulent flow conditions during the measurements can be characterized by the river depth (H), the river width (B), the mean flow velocity (V_w), the water kinematic viscosity (ν), and the shear velocity (u^*). The sampling configuration for an ADCP discharge measurement can be represented by the total number of sampled transects (N_T), the boat velocity

(V_b), the instrument sampling frequency (f), and the selected ADCP water mode which defines the noise level (σ_u) or horizontal velocity standard deviation.

[6] The following analysis focuses on the dimensionless parameter $RVar[Q]$

$$RVar[Q] = (H, B, V_w, \nu, u^*, N_T, V_b, f, \sigma_u), \quad (1)$$

but also is extended later to $RME[Q]$. Applying a key theorem in dimensional analysis, the Buckingham Pi theorem [Streeter and Wylie, 1988], the following seven dimensionless π numbers are defined using u^* (shear velocity) and H (flow depth) as independent fundamental physical quantities: $\pi_1 = N_T$; $\pi_2 = \sigma_u/u^*$; $\pi_3 = B/H$; $\pi_4 = V_w/u^*$; $\pi_5 = V_b/u^*$; $\pi_6 = Hf/u^*$; $\pi_7 = \nu/u^*H = 1/Re_\tau$, where Re_τ is a Reynolds number based on the friction velocity. Based on Buckingham's Pi theorem the relative variance of ADCP discharge measurements can be expressed as

$$RVar[Q] = F\left(N_T, \frac{\sigma_u}{u^*}, \frac{B}{H}, \frac{V_w}{u^*}, \frac{V_b}{u^*}, \frac{Hf}{u^*}, \frac{u^*H}{\nu}\right). \quad (2)$$

The dimensionless numbers π_5 and π_6 also can be rewritten as

$$\pi_5 = \frac{V_b}{u^*} = \frac{H/u^*}{H/V_b} \approx \frac{T_t}{T_c}, \quad (3)$$

$$\pi_6 = \frac{Hf}{u^*} = \frac{H/u^*}{1/f} = \frac{T_t}{\Delta t}, \quad (4)$$

where T_t is the time scale of the flow turbulence structure of size H (also named turnover time), T_c is the time the boat takes to cross a flow turbulence structure of size H and $\Delta t = 1/f$ is the sampling time interval between velocity profiles (or ensembles). Thus $RVar[Q]$ can be expressed as

$$RVar[Q] = F\left(N_T, \frac{\sigma_u}{u^*}, \frac{B}{H}, \frac{V_w}{u^*}, \frac{T_t}{T_c}, \frac{T_t}{\Delta t}, Re_\tau\right). \quad (5)$$

[7] The following assumptions were made and subsequently verified: (a) the results are not affected by using different values of the B/H ratio; (b) $Re_\tau \gg 1$ (fully developed turbulence); and (c) the ratio V_w/u^* was approximately constant. When using DNS to assess the performance of acoustic Doppler technology for characterizing turbulent flows, the noise ratio (σ_u/u^*) is not relevant for the analysis. Thus, the $RVar[Q]$ can be expressed as

$$RVar[Q] = F\left(N_T, \frac{T_t}{T_c}, \frac{T_t}{\Delta t}\right). \quad (6)$$

Preliminary analysis of the experimental data (obtained by the authors and by Oberg and Muller [2007]) shows a monotonic trend; therefore a power law is the simplest functional form that could be used. Thus, the power law has been selected in advance for the dimensional analysis. A functional form is obtained by combining the dimensionless

numbers included in equation (6) as [Streeter and Wylie, 1988]

$$RVar[Q] = a_1 \left(N_T^{b_1} \left(\frac{T_c}{T_t} \right)^{c_1} \left(\frac{T_t}{\Delta t} \right)^{d_1} \right). \quad (7)$$

Extending the analysis to $RME[Q]$,

$$RME[Q] = a_2 \left(N_T^{b_2} \left(\frac{T_c}{T_t} \right)^{c_2} \left(\frac{T_t}{\Delta t} \right)^{d_2} \right). \quad (8)$$

The parameters (a_i , b_i , c_i , d_i) for the final forms of equations (7) and (8) were obtained on the basis of fitting DNS data. Details about the mathematical and numerical models used and their validation are provided in section 3 and in Appendix A, respectively.

3. Mathematical and Numerical Models

[8] Because the main purpose of this paper is to quantify the role of flow turbulence generated by flow/bed interaction on ADCP discharge measurement uncertainties, a relatively simple case flow was simulated and analyzed: flow in a channel driven by a uniform driving force in the streamwise direction (x). The effects of bed forms (i.e., dunes), secondary currents, local scour, and sidewalls were not simulated nor analyzed in this work because these features are highly influenced by site characteristics such as topography and a universal behavior cannot be predicted.

[9] The dimensionless set of equations that govern the flow read

$$\frac{\partial \mathbf{V}}{\partial t} + \mathbf{V} \cdot \nabla \mathbf{V} = \mathbf{G} - \nabla p + \frac{1}{Re_\tau} \nabla^2 \mathbf{V}, \quad (9)$$

$$\nabla \cdot \mathbf{V} = 0, \quad (10)$$

where $\mathbf{V} = (u, v, w) = (u_x, u_y, u_z)$ is the dimensionless velocity vector, p is the dimensionless dynamic pressure, and $\mathbf{G} = (1, 0, 0)$ is the driving force (tangential component of gravity force). Dimensionless variables are defined using (a) the shear velocity $u^* = (\tau_w/\rho)^{1/2}$ as the velocity scale where τ_w is the bottom wall shear stress and ρ is the fluid density; (b) the channel height H as the length scale; (c) $T_t = H/u^*$ and (d) $P = \rho u_*^2$ are the derived scales for time and pressure, respectively. The dimensionless number in equation (9) is the Reynolds number based on the friction velocity defined as $Re_\tau = u_* H/\nu$, where ν is the dynamic viscosity, and for this work $Re_\tau = 509$, which gives a bulk Reynolds number (based on water depth and bulk streamwise velocity) $Re = V_w H/\nu = 9164$, using the ratio $V_w/u^* = 18$ computed from the available DNS data.

[10] The governing equations are solved using a dealiased pseudospectral code [Canuto et al., 1988]. Fourier expansions are employed for the flow variables in the horizontal directions (x and y are the streamwise and spanwise directions, respectively). In the inhomogeneous vertical direction (z) a Chebyshev expansion is used with Gauss-Lobatto quadrature points. An operator splitting method is used to solve the momentum equation along with the

incompressibility condition [see for example Brown et al., 2001]. First, an advection-diffusion equation is solved to compute an intermediate velocity field. After this intermediate velocity field is computed, a Poisson equation is solved to compute the pressure field. Finally, a pressure correction step is performed to obtain the final incompressible velocity field. A low-storage mixed third order Runge-Kutta and Crank-Nicolson scheme is used for the temporal discretization of the advection-diffusion terms. More details of the implementation of this numerical scheme can be found by Cortese and Balachandar [1995]. Validation of the code can be found by Cantero et al. [2007a, 2007b].

[11] The length of the simulated channel is $L_x = 4\pi H$, the width is $L_y = 4/3\pi H$, and the height is $L_z = H$. The grid resolution used is $N_x = 256 \times N_y = 256 \times N_z = 129$ and the nonlinear terms are computed in a grid $3N_x/2 \times 3N_y/2 \times N_z$ in order to prevent aliasing errors. The bottom wall represents a smooth no-slip boundary to the flow and the top wall is a free slip wall. Then, the dimensionless boundary conditions employed in the vertical direction are

$$V = 0 \text{ at } z = 0 \quad (11)$$

and

$$\frac{\partial u}{\partial z} = 0, \frac{\partial v}{\partial z} = 0, \text{ and } w = 0 \text{ at } z = 1. \quad (12)$$

[12] Periodic boundary conditions have been implemented in the two horizontal directions (implying homogeneous flow in the streamwise and spanwise directions), thus the model presented in this paper does not simulate the effect of sidewalls on the flow. Sidewall effects are relatively more important near river margins (banks) where the ADCP often cannot measure and the flow in this region is therefore estimated by extrapolating characteristics of the measured flow.

[13] The dimensionless integration time employed in this work is $T_i u_*/H = 50$ (100,000 time steps) after the flow has achieved a statistically steady state. The DNS model was validated (see Appendix A) by comparing vertical profiles of turbulence parameters for an open-channel flow with experimental results and semitheoretical curves.

4. Functional Form Obtained From DNS

[14] The parameters (a_i , b_i , c_i , d_i) of the final forms of equations (7) and (8) were obtained from analysis of the DNS-generated data. Discharges were computed from the DNS data by imitating (or simulating) an ADCP moving boat discharge measurement composed of multiple transects. The synthetic velocity data were sampled at different verticals from a simulated moving platform with a fixed frequency of 1 Hz for all the cases. Each vertical or ensemble consists of 129 velocity values. The discharge was computed for each transect by integrating velocity profiles across the cross section. The simulated ADCP measurements using the DNS differed from field ADCP measurements in that the DNS data were sampled using an idealized ADCP with one vertical beam, whereas actual ADCPs measure velocity along three or four beams that have a fixed angle in the vertical and diverge from the

ADCP with depth. Therefore in the sampling of the DNS data the velocity data are not spatially averaged and horizontal homogeneity in the velocities is assumed. Because spatial averaging would reduce the effects of turbulence fluctuations; the results presented herein will provide an upper bound for the role of flow turbulence fluctuations.

[15] Three different dimensionless times interval $T_d = \Delta t/T_t$ (equation (4)), with the same bulk $Re = 9164$ and aspect ratio $(B/H) = 4.2$, were analyzed to estimate $RVar[Q]$ and $RME[Q]$. For each dimensionless time interval ($T_d = 0.123, 0.031, \text{ and } 0.016$), the number of transects (N_T) used to obtain the measured discharge and the boat velocity (V_b) were varied. Four different values for the number of transects were used ($N_T = 1, 2, 4, \text{ and } 8$) and eight different boat velocities were analyzed. This resulted in 32 different sampling strategies (four sets of transects and eight boat velocities) for each dimensionless time interval (96 in total). Considering that $RVar[Q]$ and $RME[Q]$ are random variables for each sampling strategy, 20 data sets (sampled starting at different times in the simulation period) have been used to estimate a mean value and confidence intervals of the two parameters. Each of the 20 data sets consists in 12 transects. Thus, there are 96 mean values of $RVar[Q]$ and $RME[Q]$ values (mean values as they are the average of 20 data sets).

[16] Even though the actual flow discharge can be accurately computed from the DNS data, the mean discharge from the 12 sampled transects in each DNS data set has been assumed to be the true discharge as is the case for field measurements (true discharge is unknown [Oberg and Mueller, 2007]). The comparison between the true discharge and the mean discharge from the 12 sampled transects of the DNS data are within 1% of difference when more than four ensembles are sampled in the cross section.

[17] The selected data sets consisted of 12 transects with each transect made at the same boat speed. Percent differences were computed by subtracting the mean discharge for the 12 transects from the 1, 2, 4, 6, and 8 transect mean

discharges and dividing by the mean discharge for the 12 transect groups.

[18] The relative maximum absolute error $RME[Q]$ and the relative variance $RVar[Q]$ were computed for each data set to quantify the uncertainty in discharge measurements as

$$RME[Q] = \frac{|Q - Q_{av}|_{\max}}{Q_{av}} \text{ and } RVar[Q] = \frac{\overline{(Q - Q_{av})^2}}{Q_{av}^2},$$

respectively, where Q is the measured discharge in each transect; $|Q - Q_{av}|_{\max}$ is the maximum absolute difference in discharge from the sampled data set and Q_{av} is the average discharge of the 12 sampled transects of the data set (considered as the true discharge). $RME[Q]$ is a measure of the maximum deviation in the data set and $RVar[Q]$ represents the bulk behavior of the entire data set.

[19] Figures 1 and 2 show the histograms of $(RVar[Q])^{0.5}$ and $RME[Q]$ respectively, of the values of $(RVar[Q])^{0.5}$ and $RME[Q]$ estimated in this analysis, where $(RVar[Q])^{0.5}$ is the standard deviation of the mean flow discharge. The plotted values are averages of 20 values sampled with the same sampling configuration. The fitting performed on the values included in Figure 2 shows that $(RVar[Q])^{0.5} = 0.456(RME[Q])^{0.951}$ with $r^2 = 0.99$ being the coefficient of determination.

[20] Using the values plotted in Figures 1 and 2 and the variables defining the three dimensionless sampling times and the 32 different sampling configurations analyzed in this paper, the parameters (a_i, b_i, c_i, d_i) of the final forms of equations (7) and (8) were estimated using nonlinear regression. Table 1 shows the coefficients for each equation parameter as well as the lower and upper limit of the 95% confidence interval.

[21] The results show that the coefficients for c_2 and d_2 have similar values. The confidence intervals for c_2 and d_2

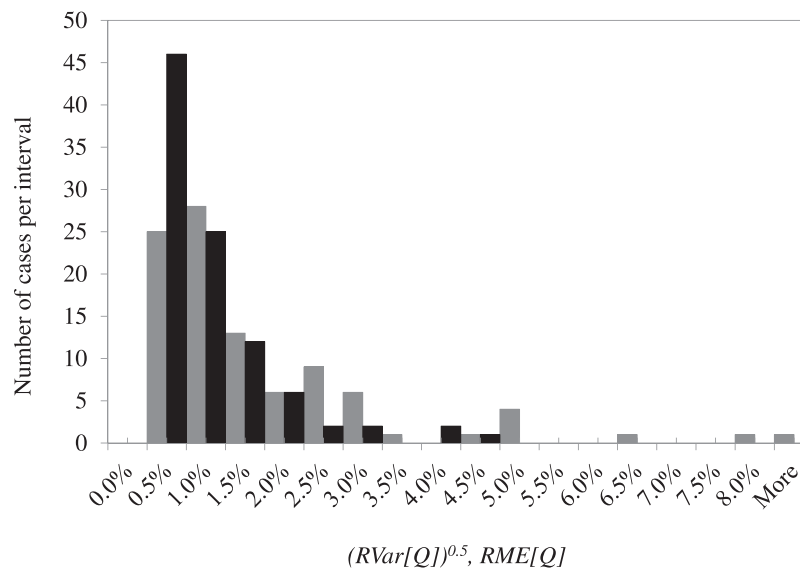


Figure 1. Histograms of $(RVar[Q])^{0.5}$ (black) and $RME[Q]$ (gray) values computed for the 96 different sampling configurations analyzed in this paper, where $(RVar[Q])^{0.5}$ is the standard deviation of the mean flow discharge.

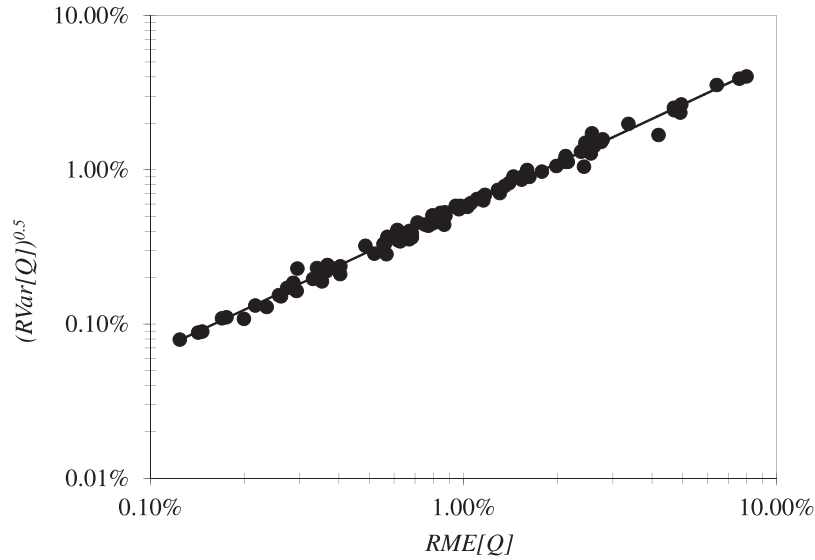


Figure 2. Correlation between values of $(RVar[Q])^{0.5}$ and $RME[Q]$ computed for the 96 different sampling configurations analyzed in this paper, where $(RVar[Q])^{0.5}$ is the standard deviation of the mean flow discharge.

also indicate that they are not statistically different. Therefore equation (8) can be expressed as

$$RME[Q] = a_4 \left(N_T^{b_4} \left(\frac{T_c}{\Delta t} \right)^{c_4} \right). \quad (13)$$

[22] On the basis of the parameters shown in Table 1 and using the 99% confidence interval, we also can consider c_1 and d_1 to be equal in value. Thus,

$$RVar[Q] = a_3 \left(N_T^{b_3} \left(\frac{T_c}{\Delta t} \right)^{c_3} \right). \quad (14)$$

A nonlinear regression was then performed to estimate the coefficients for the new parameters (a_i, b_i, c_i) of equations (13) and (14). The results of the nonlinear regression are shown in Table 2 along with the lower and upper limit of the 95% confidence interval for each parameter. Computing the ratio of equations (14) and (13), using values of the parameter a_3, b_3, c_3 and a_4, b_4, c_4 (see Table 2) which lies within the 95% confidence interval, provides an equation which is statistically similar to the relation, $RVar[Q] = 0.21RME[Q]^{1.9}$ derived from the equation $(RVar[Q])^{0.5} = 0.456(RME[Q])^{0.951}$ presented before. The ratio of equations (14) and (13) (where mean values of the parameters

are used from Table 2) shows differences that arise because of the different variables involved in the nonlinear fitting process.

[23] Thus, equations (14) and (13) can be expressed, respectively, as

$$RVar[Q] = 0.00038 \left(N_T \left(\frac{T_c}{\Delta t} \right)^{0.66} \right)^{-1.41}, \quad (15)$$

$$RME[Q] = 0.039 \left(N_T \left(\frac{T_c}{\Delta t} \right)^{0.55} \right)^{-0.79}. \quad (16)$$

The evolution of both $RVar[Q]$ and $RME[Q]$ for the different sampling configurations varying the total number of sampled transect (N_T) and the boat velocity (V_b) for each dimensionless sampling time are shown in Figures 3 and 4. The dimensionless numbers shown on the abscissa for each plot are values of $N_T(T_c/\Delta t)^x$, with x being the ratio of coefficients c_3/b_3 and c_4/b_4 for equations (15) and (16), respectively, from Table 2. The variables N_T and T_c are directly related to the exposure time for ADCP discharge measurements from moving platforms. The optimum exposure time can be obtained by either increasing the number of sampled transects (N_T) or slowing down the boat speed

Table 1. Parameters of Equations (7) and (8) Obtained From Nonlinear Regression of DNS Data

$RVar[Q]$, Equation (7)				$RME[Q]$, Equation (8)			
Parameter	Mean	95% Confidence Interval		Parameter	Mean	95% Confidence Interval	
		Lower Limit	Upper Limit			Lower Limit	Upper Limit
a_1	0.00023	0.00020	0.00026	a_2	0.030	0.025	0.034
b_1	-1.39	-1.48	-1.31	b_2	-0.79	-0.86	-0.73
c_1	-0.94	-0.99	-0.88	c_2	-0.43	-0.46	-0.40
d_1	-0.78	-0.85	-0.72	d_2	-0.35	-0.40	-0.30

Table 2. Parameters of Equations (13) and (14) Obtained From Nonlinear Regression of DNS Data

<i>RVar[Q]</i> , Equation (14)				<i>RME[Q]</i> , Equation (13)			
Parameter	Mean	95% Confidence Interval		Parameter	Mean	95% Confidence Interval	
		Lower Limit	Upper Limit			Lower Limit	Upper Limit
a_3	0.00038	0.00034	0.00042	a_4	0.039	0.037	0.041
b_3	-1.41	-1.54	-1.29	b_4	-0.79	-0.86	-0.72
c_3	-0.93	-1.01	-0.86	c_4	-0.43	-0.46	-0.40

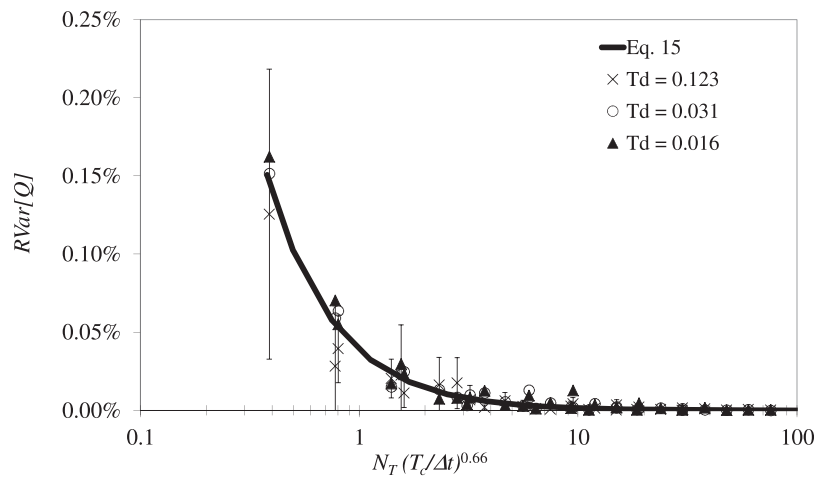


Figure 3. Evolution of *RVar[Q]* for the different sampling configurations. The best fit curve of all the simulated data is represented by equation (15).

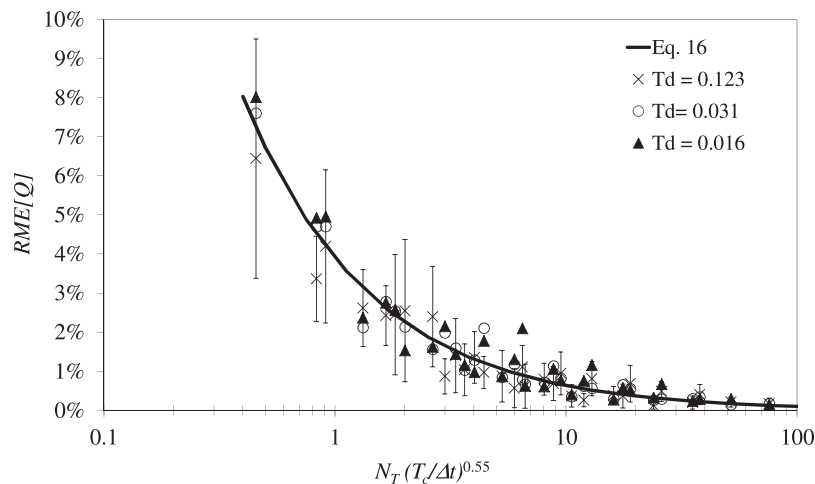


Figure 4. Evolution of *RME[Q]* for the different sampling configurations. The best fit curve of all the simulated data is represented by equation (16).

Table 3. Names and Locations for the Sites Used in This Study

Site Description	Site ID	Latitude	Longitude	Drainage Area (km ²)
Fox River at Montgomery, IL, USA	FoxMon	41.73	-88.33	4,490
Mississippi River at Chester, IL, USA	Chester	37.9	-89.84	1,840,000

(increasing T_c). On the other hand, Δt indicates the effect of the sampling frequency affecting the total number of sampled profiles. *Garcia et al.* [2012] showed that the measurement exposure time (sometimes called duration), and sampling frequency are critical factors in reducing discharge measurement uncertainty. In equations (15) and (16), the exponent for N_T and the exponent for the ratio ($T_c/\Delta t$) are different, with the exponent for the ratio ($T_c/\Delta t$) being smaller. This indicates that increasing the number of transects has a greater impact in reducing ADCP discharge measurement uncertainty caused by turbulent fluctuations than increasing the sampling frequency or decreasing the boat velocities, due to the correlation structure of the turbulence flow field. Increasing N_T increases the number of independent samples.

[24] The values included in Figures 3 and 4 are the means of the 20 data sets for each sampling configuration. In addition, the 95% confidence intervals are shown for both $RVar[Q]$ and $RME[Q]$ for flow conditions represented by $T_d = 0.123$. The best fit curve of all the simulated data for equations (15) and (16) are shown in Figure, 3 and 4, respectively. Both uncertainty estimates of mean flow discharge, $RVar[Q]$ and $RME[Q]$, decrease as N_T and T_c increase. For the same flow condition a greater value for T_c implies a lesser value for V_b .

5. Validation of Functional Forms Using Field Measurements

[25] The functional forms obtained using DNS data for both uncertainty parameters $RVar[Q]$ and $RME[Q]$ were validated using field data, along with the hypotheses included in the dimensional analysis. Field data from natural streams having a relatively wide range of flow and sampling conditions were selected for this validation.

[26] Because only random errors (uncertainty) of discharge measurements due to the presence of flow turbulence can be analyzed using DNS data, a detailed analysis of the available field data was performed in order to select the optimum set for use in the validation process. Data sets of field measurements were chosen such that instrument and environmental noise was minimized. The discharge measurement sites chosen for this study are shown in

Table 3, and the main parameters describing the measuring conditions for each data set are summarized in Table 4.

[27] Two 600 kHz ADCPs, manufactured by Teledyne RD Instruments (downlooking configuration from moving platforms) were used for the discharge measurements. The sampling conditions and the instrument configuration were different in each data set (Table 5). At the Fox River at Montgomery, measurements were made with a high resolution, pulse coherent mode (water mode 11) and a tethered boat and rope-and-pulley system to control the boat speed. At the Mississippi River at Chester, measurements were made using water mode 1 and a larger (6 m) manned boat.

[28] The sites selected in this study present different aspect ratio (B/H) values, different Re numbers, and different noise level σ_u (see Tables 4 and 5) from the conditions simulated using DNS in order to validate the hypotheses that were assumed in the dimensional analysis: (a) the results are not affected by using different values of the B/H ratio; (b) $Re_\tau \gg 1$ (fully developed turbulence); and (c) the ratio V_w/u^* was approximately constant and equal to 18.

[29] Each data set summarized in Table 5 consists of data from 12 transects at the same location. Every selected set of field data (12 transects each) was analyzed using the same methodology described for the DNS data. Thus, the mean discharge from 12 transects is assumed to be the true discharge and the $RVar[Q]$ and the $RME[Q]$ associated with 1, 2, 4, and 8 consecutive transects were computed as the relative variance and the relative maximum absolute error of the available discharge samples in each data set.

[30] There is good agreement between the values of $RVar[Q]$ and $RME[Q]$ developed from DNS and that computed from field data (Figures 5 and 6). The differences between $RVar[Q]$ estimated from DNS data and $RVar[Q]$ computed from field data are most likely due to the presence of other random processes that affect the measurement (e.g., Doppler noise, environmental noise, etc.). The values of the aspect ratio B/H analyzed in this paper range from 4 for the DNS data to 23.4 for FoxMon and 78.8 for Chester. The functional form estimated with the DNS data represents a lower bound of the expected uncertainties in field ADCP discharge measurements.

[31] The dimensionless curves from equations (15) and (16) can be used to quantify the role of the presence of flow turbulence fluctuations on uncertainties of ADCP discharge measurements. However, equations (15) and (16) are not formulated as a tool for estimating ADCP discharge measurement uncertainties from *all* error sources. The effects of instrument noise and environmental noise are not reflected in the coefficients of equations (15) and (16). The results of this work indicate that random errors due to flow turbulence are large when measuring in shallow flows ($H < \sim 0.5$ m) and when boat velocities for the ADCP discharge measurement are relatively large. In order to illustrate this,

Table 4. Summary of Flow Conditions for Each Site

Site ID	Total Discharge Q (m ³ s ⁻¹)	Measured Discharge Q_m (m ³ s ⁻¹)	Width B (m)	Area A (m ²)	Mean Water Velocity V_w (m s ⁻¹)	Mean Depth H (m)	B/H	Reynolds Number Re	Froude Number Fr
FoxMon	17.1	10.6	44.6	85	0.20	1.91	23.4	3.8E+05	0.05
Chester	3270.0	2347.4	487.6	3016	1.08	6.19	78.8	6.7E+06	0.14

Table 5. Description of the Data Sets Collected at Each Site

Site and Date	Data Set	Average Number of Ensembles Per Transect N	Average Exposure Time Per Transect T (s)	Average Boat Speed $\sigma_u V_b$ (m s^{-1})	Noise Level (m s^{-1})
FoxMon Date: 03/07/2007	1	479	191.1	0.24	0.01*
	2	379	151.1	0.30	0.01*
	3	247	98.5	0.47	0.01*
Chester Date: 18/09/2001	1	807	496.8	1.01	0.14
	2	773	475.5	1.08	0.14
Sampling Configuration Information For All Transects/Sites 0.25 m Blanking distance, 1 Water ping, 1 Bottom ping, Bottom Mode 5					
Site Specific Sampling Configuration Information					
FoxMon	600 kHz ADCP, Water mode 11, 0.10 m Bin size, 0.09 m ADCP depth, $f = 2.5$ Hz.				
Chester	*Written communication (D. Mueller, USGS) for $H < 2$ m. 600 kHz ADCP, Water mode 1 ($WV = 1.88 \text{ m s}^{-1}$), 0.50 m Bin size, 0.35 m ADCP Depth, $f = 1.62$ Hz.				

critical boat velocities (maximum mean velocities) were computed using equations (15) and (16) and using $V_b = H/T_c$ (see equation (3)) for three different levels of uncertainty due to flow turbulence. Table 6 shows critical boat velocities for values of $(RVar[Q])^{0.5}$ and $RME[Q]$ of less than or equal to 1%, 2%, and 3%; and assuming at least two transects are sampled ($N_T = 2$) with a sampling interval $\Delta t = 1$ s. For example, values of $(RVar[Q])^{0.5}$ greater than 1% will be observed when measuring a 1 m deep flow with two transects and boat velocities are greater than 0.68 m s^{-1} . On the other hand, values for the maximum relative error (defined by $RME[Q]$) greater than 1% will be observed when measuring a 2 m deep flow, with two transects and boat velocities are greater than 0.30 m s^{-1} (Table 6). Even though the sampling frequency cannot be modified in the ADCP sampling configuration after the optimum water mode is defined, these results show that increasing the sampling frequency by 2 will have the same effect as decreasing the boat velocity by one-half.

[32] Thus, Table 6 shows that the $(RVar[Q])^{0.5}$ values due to flow turbulence are less than 3% for the most common sampling and flow conditions usually sampled during discharge measurements when at least two transects are sampled. On the other hand, it is possible for the $RME[Q]$ due to flow turbulence to exceed 3% in shallow flows ($H < 0.5$ m).

6. Conclusions

[33] This work presents a systematic analysis quantifying the role of flow turbulence fluctuations on uncertainties of acoustic Doppler current profilers (ADCP) discharge measurements from moving boats. Data sets of three-dimensional flow velocities with high temporal and spatial resolution were generated from direct numerical simulation (DNS) of turbulent open channel flow. DNS presents an ideal tool to generate such a detailed data set because: (a) only contribution due to the presence of flow turbulence

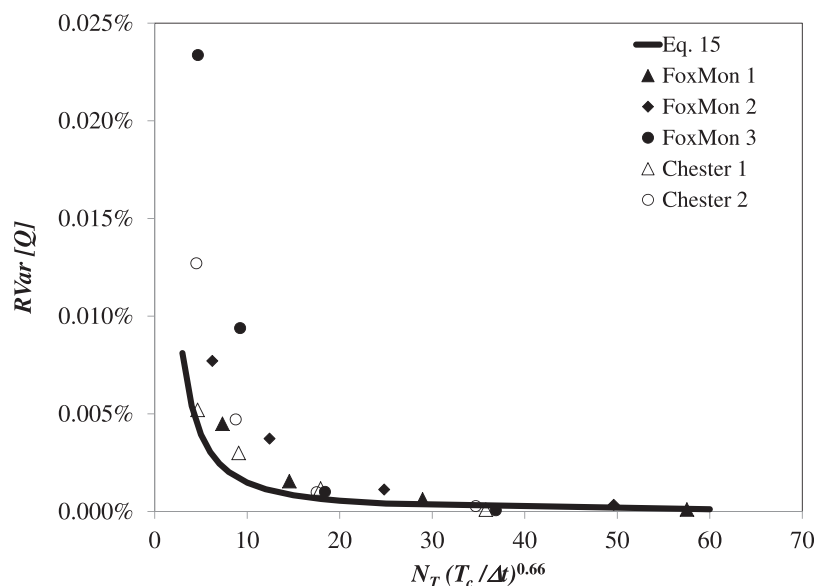


Figure 5. $RVar[Q]$ values estimated from numerical simulation (DNS, equation (15)) and field data (Fox River at Montgomery, IL and Mississippi River at Chester, IL).

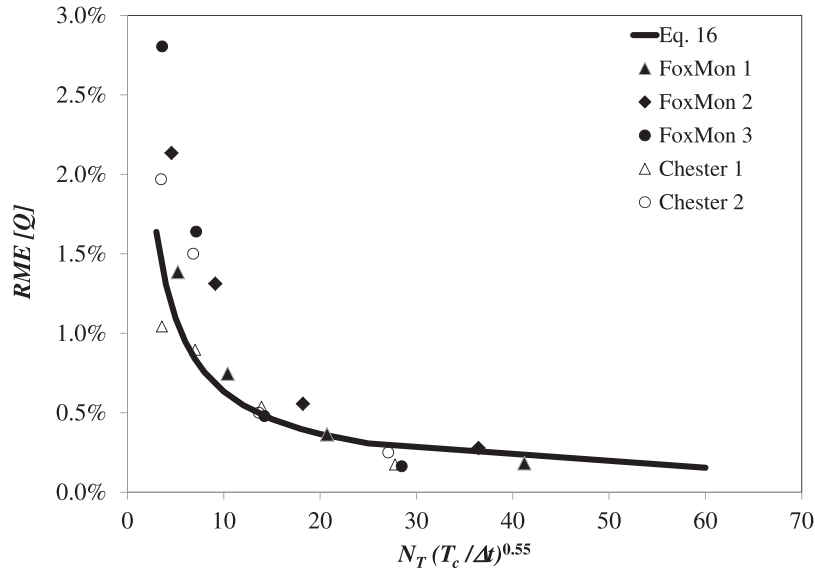


Figure 6. $RME[Q]$ values estimated from numerical simulation (DNS, equation (16)) and field data (Fox River at Montgomery, IL and Mississippi River at Chester, IL).

fluctuations are included in the analysis and (b) the simulation solves for all relevant time and length scales present in the flow with no need for turbulence closure schemes. Although DNS can hardly be applied to field-scale flows, the levels of turbulence attained at moderate Reynolds number flows where DNS is feasible are representative of mature turbulent flows. Dimensionless functions relating dimensionless parameters quantifying the uncertainty (relative variance and relative maximum random error) due to flow turbulence as a function of appropriately defined dimensionless sampling configuration and flow conditions parameters were developed and validated with field-scale discharge measurements. These results show that increasing the number of transects has a stronger impact on reducing the role of turbulence fluctuations on uncertainties of ADCP discharge measurements than increasing the sampling frequency and decreasing the boat velocities. This owes to the correlation structure of the turbulent flow field, and it is most likely because increasing N_T increases the number of independent samples. In addition, the results of this work indicate that random errors due to the flow turbulence become large when measuring in shallow flows ($H < 0.5$ m) with relatively large boat velocities.

Table 6. Critical Boat Velocities (m s^{-1}) (Maximum Velocities) Acceptable for Uncertainty Levels Due to Flow Turbulence (Defined by $(RVar[Q])^{0.5}$ and $RME[Q]$) Less Than or Equal to 1%, 2%, and 3%, Assuming $N_T = 2$ and $\Delta t = 1$ s

H (m)	$(RVar[Q])^{0.5}$			H (m)	$RME[Q]$		
	1%	2%	3%		1%	2%	3%
0.50	0.34	1.51	3.61	0.50	0.08	0.38	0.97
1.00	0.68	3.02	7.23	1.00	0.15	0.76	1.94
2.00	1.36	6.04	14.46	2.00	0.30	1.51	3.88

Appendix A

[34] The DNS model presented in section 3 was validated by comparing vertical profiles of turbulence parameters for an open-channel flow with experimental results [Nezu, 1977; Nezu and Nakagawa, 1993] and semitheoretical curves [Nezu and Rodi, 1986; Nezu and Nakagawa, 1993].

[35] Mean velocity profiles are obtained by time-averaging the instantaneous horizontal plane averages. Using the same approach, turbulence parameter profiles are estimated by using instantaneous horizontal plane perturbations from the mean variable. Figure A1 shows the vertical profiles of mean streamwise dimensionless velocity $u^+ = u/u_*$. Also shown is the law of the wall for open channel flows [Nezu and Nakagawa, 1993]:

$$u^+ = \frac{u}{u_*}, \quad z^+ = \frac{zu_*}{\nu}, \quad (\text{A1})$$

which is valid for the viscous sublayer ($z^+ < 5$), and the log-law

$$u^+ = \frac{1}{\kappa} \ln(z^+) + A, \quad (\text{A2})$$

which is inherently valid in the wall region ($0.1 < z/H < 0.3$). According to Pope [2000] the latter is equivalent to the range $50 < z^+ < 153$, for $Re_\tau = 509.1$. Nezu and Rodi [1986] showed that for smooth open channel flow, the Von Karman constant (κ) and the integral constant A have the universal values of 0.41 and 5.29, respectively. Nezu and Nakagawa [1993] accounted for the observed deviation from the log-law for $z/H > 0.3$ by adding a wake function. A very good agreement is observed between the simulated data using DNS and the theoretical velocity distributions for each region.

[36] Vertical profiles of the dimensionless velocity root mean square for the streamwise (u'), spanwise (v'), and vertical (w') components were computed from DNS data and

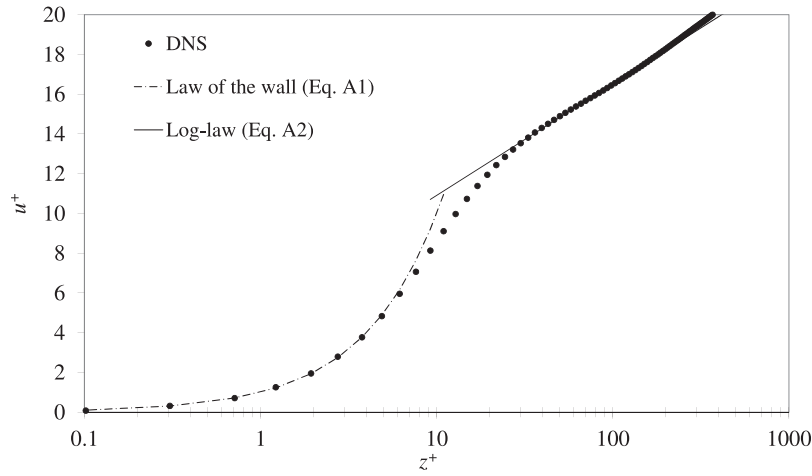


Figure A1. Vertical profile of mean streamwise dimensionless velocity ($u^+ = u/u^*$ and $z^+ = zu^*/\nu$).

are shown in Figures A2, A3, and A4, respectively. These profiles were compared to experimental data measured in earlier work for smooth, open channel flows [Nezu, 1977] and semitheoretical relations. Semitheoretical relations for dimensionless turbulent intensities were presented by Nezu and Nakagawa [1993]:

$$\frac{u'}{u_*} = D_u \exp\left(-\frac{z}{H}\right), \quad (\text{A3})$$

$$\frac{v'}{u_*} = D_v \exp\left(-\frac{z}{H}\right), \quad (\text{A4})$$

$$\frac{w'}{u_*} = D_w \exp\left(-\frac{z}{H}\right), \quad (\text{A5})$$

where D_u , D_v , and D_w are empirical constants. They are valid in the log-law region [$0.1 < z/H < 0.3$ for $Re_\tau = 509.1$ [Pope 2000], where the turbulent energy is in equilibrium (the rate of the turbulent energy production is equal to the

rate of turbulent dissipation). Nezu [1977] analyzed hot-film data and determined values for these empirical constants such that $D_u = 2.30$, $D_v = 1.63$, and $D_w = 1.27$, which proved to be independent of the Reynolds number and Froude numbers.

[37] Near the wall $z^+ < 50$ ($z/H < 0.1$ for the analyzed Re_τ), the turbulent generation and dissipation are not in equilibrium. Nezu and Nakagawa [1993] suggested that in this region, empirical formulas for the dimensionless root mean square of the water velocity in the streamwise region are more useful for correlating data near the wall. They presented the following empirical relation:

$$\frac{u'}{u_*} = 0.3z^+. \quad (\text{A6})$$

[38] Nezu and Nakagawa [1993] also suggested that the distribution of dimensionless root mean square of water velocity for the streamwise direction (u') has a maximum for $z^+ = 10-20$ ($z/H = 0.02-0.04$ for the analyzed Re_τ).

[39] Figure A5 shows a comparison between the vertical profiles of dimensionless turbulent kinetic energy (TKE)

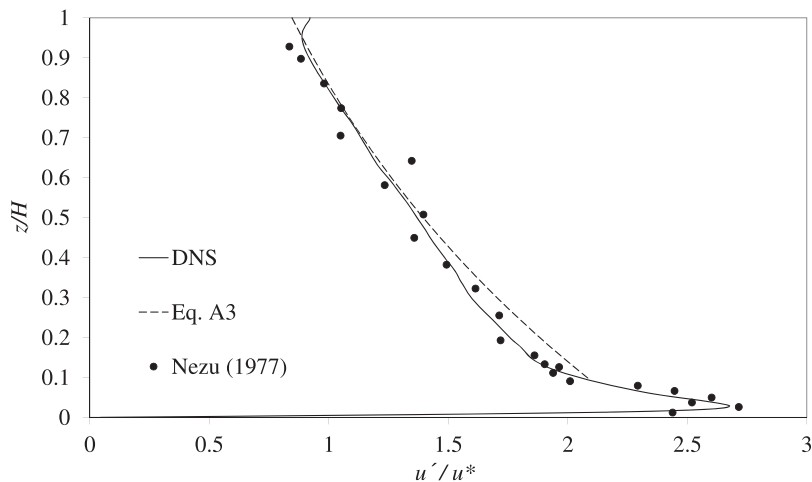


Figure A2. Dimensionless root mean square of water velocity for the streamwise direction (u').

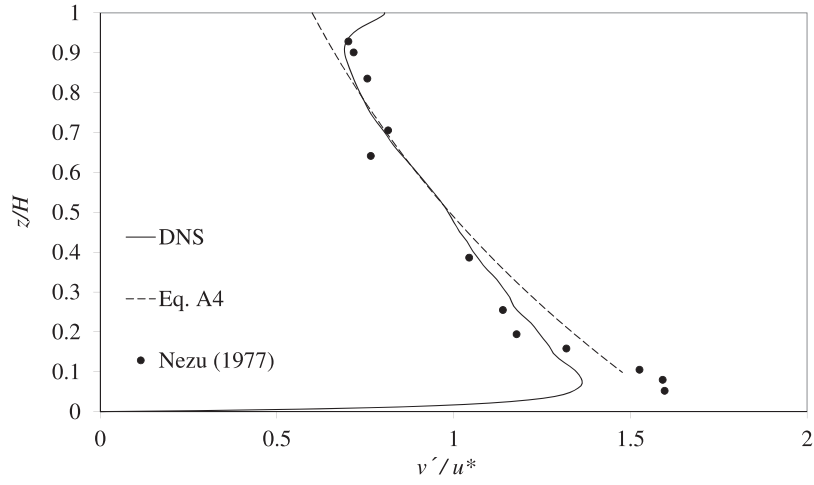


Figure A3. Dimensionless root mean square of water velocity for the spanwise direction (v').

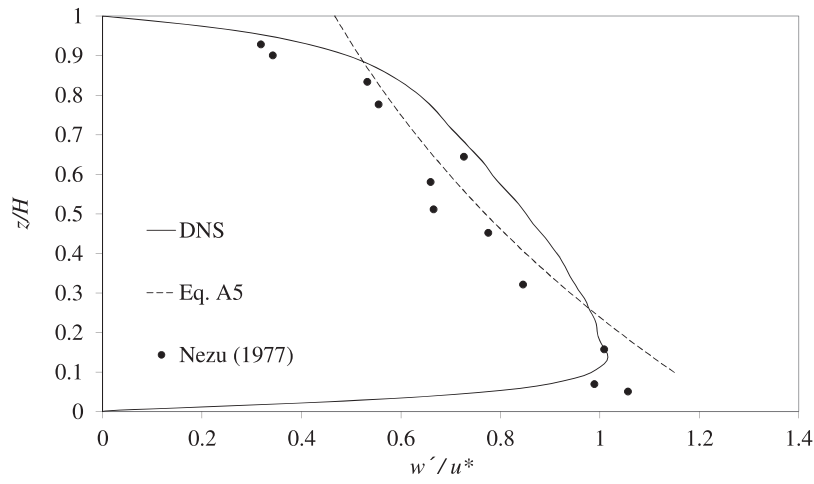


Figure A4. Dimensionless root mean square of water velocity for the vertical direction (w').

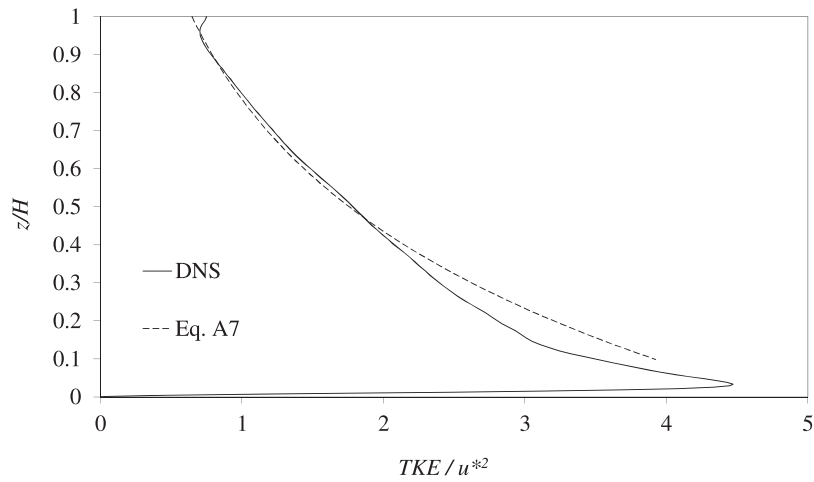


Figure A5. Dimensionless turbulent kinetic energy.

computed from DNS data and the semitheoretical relation proposed by *Nezu and Nakagawa* [1993] for the region where the turbulent energy is in equilibrium:

$$\frac{TKE}{u_*} = D \exp\left(-2 \frac{z}{H}\right). \quad (A7)$$

[40] *Nezu* [1977] analyzed hot-film data and determined a value for this empirical constant $D = 4.78$.

[41] **Acknowledgment.** We gratefully acknowledge the funding from the USGS through the Office of Surface Water. Use of trade, product, or firm names in this paper is for descriptive purposes only and does not imply endorsement by the U.S. Government.

References

- Abe, H., H. Kawamura, and Y. Matsuo (2001), Direct numerical simulation of a fully developed turbulent channel flow with respect to the Reynolds number dependence, *J. Fluids Eng.*, *123*(2), 382–393.
- Brown, D., R. Cortez, and M. Minion (2001), Accurate projection methods for the incompressible Navier–Stokes equations, *J. Comput. Phys.*, *168*(2), 464–499.
- Cantero, M., J. Lee, S. Balachandar, and M. García (2007a), On the front velocity of gravity currents, *J. Fluid. Mech.*, *586*, 1–39.
- Cantero, M., S. Balachandar, and M. García (2007b), High resolution simulations of cylindrical density currents, *J. Fluid. Mech.*, *590*, 437–469.
- Canuto, C., M. Y. Hussaini, A. Quarteroni, and T. A. Zang (1988), *Spectral Methods in Fluid Dynamics*, Springer, New York.
- Cortese, T., and S. Balachandar (1995), High performance spectral simulation of turbulent flows in massively parallel machines with distributed memory, *Int. J. High Performance Comput. Appl.*, *9*(3), 187–204.
- García, C., M. Cantero, Y. Niño, and M. García (2005), Turbulence measurements using acoustic Doppler velocimeter, *J. Hydraul. Eng.*, *131*(12), 1062–1073.
- García, C. M., L. Tarrab, K. Oberg., R. Szupiany and M. Cantero (2012), Variance of discharge estimates sampled using acoustic Doppler current profilers from moving platforms, *J. Hydraul. Eng.*, in press.
- Nezu, I. (1977), Turbulence structure in open channel flows, Ph.D Thesis, Kyoto University, Kyoto, Japan.
- Nezu, I., and H. Nakagawa (1993) *Turbulence in Open Channels*, AA Balkema, Rotterdam, The Netherlands.
- Nezu, I., and W. Rodi (1986), Open-channel flow measurements with a laser Doppler anemometer, *J. Hydraul. Eng.*, *112*(5), 335–355.
- Oberg, K., and D. Mueller (2007), Validation of streamflow measurements made with acoustic Doppler current profilers, *J. Hydraul. Eng.*, *133*(12), 1421–1432.
- Oberg, K., S. Morlock, and W. Caldwell (2005), Quality-assurance plan for discharge measurements using acoustic Doppler current profilers, *U.S. Geol. Surv. Sci. Invest. Rep.*, 2005-5183.
- Pope, S. B. (2000), *Turbulent Flows*, Cambridge University Press, Cambridge.
- Streeter V., and B. Wylie (1988), *Fluid Mechanics*, 8th ed., McGraw-Hill, New York.